Oversampled Receiver for Coded OTFS With Different D/A Reconstruction Filters

Preety Priya, *Member, IEEE*, Yi Hong, *Senior Member, IEEE*, and Emanuele Viterbo, *Fellow, IEEE*

***Abstract*—This letter analyzes a coded OTFS system with different digital-to-analog (D/A) reconstruction filters and an oversampling receiver in the presence of fractional delay and Doppler. In such a setting, we present the input-output relation for a generic D/A reconstruction filter. Then we present the low complexity delay time (DT) maximal ratio combining (MRC) detection with receiver oversampling for coded OTFS with turbo iteration. Further, we focus on two D/A reconstruction filters for OTFS: Sinc and root raised cosine (RRC) and we provide, for the first time, a fair comparison of their performance in terms of bandwidth expansion, spectral efficiency, and out-of-band (OOB) radiation. For this, we fix the spectral efficiency for all cases by tuning the code rate and the roll-off factor. Under the same spectral efficiency, we conclude that the Sinc filter outperforms the RRC filter in terms of error performance and bandwidth requirement for both oversampling and Nyquist rate sampling receivers.**

***Index Terms*—Coded OTFS, reconstruction filter, oversampling, OOB, MRC detection.**

I. Introduction

THE LANDSCAPE of future wireless communications is witnessing a paradigm shift in research driven by the increasing demand for high mobility applications. Recently, a new waveform orthogonal time frequency space (OTFS) [1], [2] has emerged as a superior alternative to the conventional orthogonal frequency division multiplexing (OFDM), in scenarios with high Doppler spreads. In OTFS, the information symbols are multiplexed in the delay-Doppler (DD) domain rather than the time-frequency domain used in OFDM. The channel response in DD domain captures the dominant scattered paths with their distinct gain, delay, and Doppler, which simplifies the channel estimation and equalization complexity.

Extensive research on channel estimation (CE) and detection have been explored in the literature (see [2], [3], [4], [5], [6], [7], [8], [9], [10], [11], [12], [13] and references therein). Most of them are based on Nyquist rate sampling receiver. More recently, in [14], receiver oversampling for OTFS has been investigated, where message passing (MP) detection were adopted. In [15], receiver oversampling with maximal ratio combining (MRC) detection was shown to improve bit error rate (BER) performance.

However, most of the existing works ignore the effects of the digital-to-analog (D/A) reconstruction filter which is implicitly included in the transmit pulse $g_{\rm tx}(t)$ (of duration $T = MT_s$) of the Heisenberg transform [1]. The out-of-band (OOB) emissions beyond the bandwidth B of the transmitted signal is specifically affected by the D/A reconstruction filter impulse response $p_{\rm tx}(t)$ applied to the Nyquist rate samples spaced by $T_s = 1/B$.

In this letter, we analyze a coded discrete Zak transform-based OTFS system with different D/A reconstruction filters and receiver oversampling. Specifically, we explore the performance implications of two types of reconstruction filters i) Sinc filter and ii) root raised cosine (RRC) filter in terms of bandwidth expansion, spectral efficiency, and OOB radiation. For OOB evaluation, we consider the truncated reconstruction filters with limited span.

To ensure a fair BER comparison, we fix the same spectral efficiency across all cases, and accordingly set the code rate, and roll off factor. This fair comparison was never presented in the OTFS literature.

Under this configuration, we present the input-output relationship for a generic D/A reconstruction filter with receiver oversampling. Then, we present a low complexity delay time (DT) MRC detection with an arbitrary D/A reconstruction filter for coded OTFS with turbo iteration. Finally, we evaluate the performance in terms of OOB radiation and BER through simulations. We conclude that, under same spectral efficiency, Sinc and RRC filters result in equivalent bandwidth requirement and error performance for oversampling receiver, but Sinc outperforms RRC with Nyquist rate sampling receiver.

Notations: x, $\mathbf{x}$, $\mathbf{X}$ represent scalar, vector, and matrix, respectively; $(\cdot)^T$, $(\cdot)^H$, $(\cdot)^*$, $*$, $\circledast$, $\circ$, and $\oslash$, denote the transpose, Hermitian, conjugate, linear convolution, circular convolution, Hadamard product, and Hadamard division, respectively; $\mathbf{X}[m, n]$ represents element in m-th row and n-th column of matrix $\mathbf{X}$; and $\mathbf{x}[n]$ denotes n-th element of vector $\mathbf{x}$; $\text{vec}(\mathbf{A})$ denotes the column vectorization of matrix $\mathbf{A}$; $\text{vec}^{-1}(\mathbf{a})$ denotes the inverse operation of vectorization; $\mathbb{Z}$ denotes the integer numbers; $\mathcal{L}$ represents a set and $|\mathcal{L}|$ is the cardinality of set $\mathcal{L}$; δ is the Dirac-delta operator; $\mathbf{F}_M$ is the M-point normalized discrete Fourier transform (DFT) matrix

Manuscript received 28 April 2024; accepted 24 May 2024. Date of publication 28 May 2024; date of current version 11 September 2024. This was supported by the Australian Research Council through the Discovery Project under Grant DP200100096. The associate editor coordinating the review of this article and approving it for publication was D. P. Moya Osorio. *(Corresponding author: Emanuele Viterbo.)*

Preety Priya is with the Department of Electronics and Communication Engineering, National Institute of Technology Calicut, Kozhikode 673601, India (e-mail: preetypriya@nitc.ac.in).

Yi Hong and Emanuele Viterbo are with the Department of Electrical and Computer Systems Engineering, Monash University at Clayton, Clayton, VIC 3800, Australia (e-mail: yi.hong@monash.edu; emanuele.viterbo@monash.edu).

Digital Object Identifier 10.1109/LWC.2024.3406612

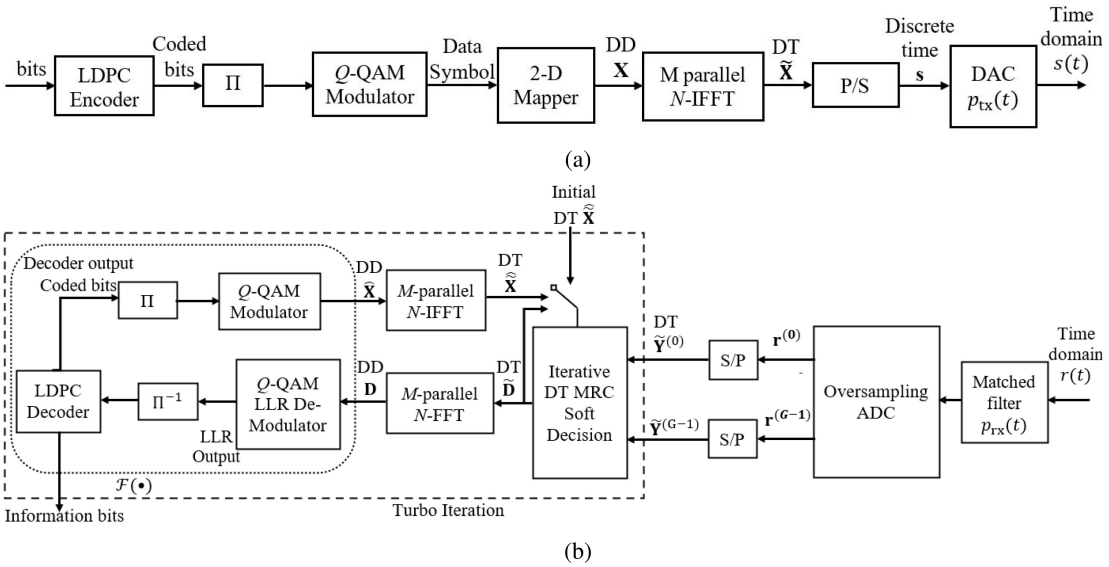

Fig. 1. Coded OTFS with Reconstruction Filter (a) Transmitter (b) Oversampled Receiver.

with its entries as $\mathbf{F}_M[m,n] = \frac{1}{\sqrt{M}} e^{-j2\pi mn/M}$; a circulant matrix is defined as

$$\text{circ}(\mathbf{a}) = \begin{bmatrix} a[0] & a[N-1] & \dots & a[1] \\ a[1] & a[0] & \dots & a[2] \\ \vdots & \vdots & \ddots & \vdots \\ a[N-1] & a[N-2] & \dots & a[0] \end{bmatrix}.$$

II. System Model

We consider a low-density parity check (LDPC) coded OTFS system, as illustrated in Fig. 1, where an OTFS frame signal nominally occupies a bandwidth of $B = M\Delta f$ and has a duration of $T_f = NT$. Here, M represents the number of subbands of size $\Delta f = \frac{1}{T}$, where T denotes the block duration, and N denotes the number of blocks forming the OTFS frame, i.e., an OTFS frame contains N blocks where each block has M samples. In this letter, we will utilize zero-padding OTFS [15].

We assume that the information bit sequence is encoded using an LDPC of rate R_c, then interleaved and mapped to complex symbols using a Q-QAM modulator. These QAM symbols are then arranged into a two-dimensional DD grid forming a DD matrix $\mathbf{X} = [\mathbf{x}_0, \dots, \mathbf{x}_{M-1}]^T \in \mathbb{C}^{M\times N}$, where $\mathbf{x}_m \in \mathbb{C}^{N\times 1}$ is the m-th row of $\mathbf{X}$ for $m \in [0, M-1]$, representing the DD vector at m-th delay index. It is then passed through an inverse discrete Zak transform (IDZT) to obtain the discrete time sample vector [2]

$$\mathbf{s} \triangleq \{\mathbf{s}[q]\}_{q=0}^{MN-1} = \text{IDZT}(\mathbf{X}) = \text{vec}\left(\mathbf{X}\mathbf{F}_N^H\right) = \text{vec}\left(\tilde{\mathbf{X}}\right), \quad (1)$$

where $\tilde{\mathbf{X}} = [\tilde{\mathbf{x}}_0, \dots, \tilde{\mathbf{x}}_{M-1}]^T = \mathbf{X}\mathbf{F}_N^H \in \mathbb{C}^{M\times N}$ is the DT matrix representation of the OTFS frame, and $\tilde{\mathbf{x}}_m$ is the m-th row of $\tilde{\mathbf{X}}$, representing the DT vector at m-th delay index. Considering the Nyquist sampling rate $f_s = \frac{1}{T_s} = B$, where T_s is the Nyquist sampling interval, the discrete-time samples are converted to continuous time using D/A reconstruction filter with impulse response $p_{\text{tx}}(t)$ as [16]

$$s(t) = \sum_{q=0}^{MN-1} \mathbf{s}[q]\, p_{\text{tx}}\left(\frac{t}{T_s} - q\right). \quad (2)$$

Note that the reconstruction filter impulse response $p_{\text{tx}}(t)$ in discrete Zak transform based OTFS is related to the pulse shaping waveform $g_{\text{tx}}(t)$ utilized in the Heisenberg transform in the original OTFS proposed by Hadani [1] as

$$g_{\text{tx}}(t) = \sum_{m=0}^{M-1} p_{\text{tx}}(t - mT_s). \quad (3)$$

Then the time domain signal $s(t)$ is transmitted through a multipath time-varying channel of L paths with maximum delay and Doppler shifts $\tau_{\max}$, $\nu_{\max}$, satisfying $\tau_{\max}\nu_{\max} \ll 1$ (i.e., an underspread channel). The i-th path, $i \in [0, L-1]$, has path gain h_i, delay and Doppler shifts, τ_i, ν_i, respectively. Then the DD channel response can be expressed as

$$h(\tau,\nu) = \sum_{i=0}^{L-1} h_i \delta(\tau - \tau_i)\delta(\nu - \nu_i). \quad (4)$$

The channel impaired received signal can be expressed as

$$r(t) = \sum_{i=0}^{L-1} h_i\, e^{j2\pi\nu_i(t-\tau_i)} s(t-\tau_i) + w(t), \quad (5)$$

where $w(t)$ is the time-domain additive noise. The received signal is first processed through a matched filter, $p_{\text{rx}}(t)$, and then it is sampled to convert it in the discrete time domain. We consider an oversampling receiver with oversampling factor G.

Let $p(t) = p_{\text{tx}}(t) * p_{\text{rx}}(t)$ is the equivalent filter response that includes bandlimiting D/A reconstruction filters utilized by both the transmitter and receiver to control signal bandwidth and to reject OOB interferences.

We let $l_i = MG\Delta f \tau_i$ and $k_i = NT\nu_i$ be the *normalized delay* and *normalized Doppler* (not necessarily integers), respectively, and $l_{\max}$, $k_{\max}$ be the normalized delay and

Doppler indices associated with $\tau_{\max}$, $\nu_{\max}$, respectively. Substituting (2) in (5), along with some mathematical manipulation, we can express the oversampled received signal sampled at $t = qT_s + \frac{g}{G}T_s$, for $g \in [0, G-1]$, and $q \in [0, MN-1]$ as

$$r\Big(qT_s + \frac{g}{G}T_s\Big) = \sum_{l\in\mathcal{L}} h\Big(qT_s + \frac{g}{G}T_s, l\Big)s[q-l] + w\Big(qT_s + \frac{g}{G}T_s\Big), \tag{6}$$

where

$$h\Big(qT_s + \frac{g}{G}T_s, l\Big) = \sum_{i=0}^{L-1} h_i e^{j\frac{2\pi}{MN}k_i\left(q+\frac{g}{G}-\frac{l_i}{G}\right)} p\Big(l + \frac{g}{G} - \frac{l_i}{G}\Big) \tag{7}$$

represents the discrete-time baseband channel at l-th tap with g-th phase offset by gT_s/G, sampled at qT_s, which includes the sampled equivalent filter response $p(l + \frac{g}{G} - \frac{l_i}{G})$ of the transmitter and receiver. Further, $w(qT_s + \frac{g}{G}T_s)$ denotes the sampled additive noise and $\mathcal{L}$ is the set containing dominant channel taps l greater than a certain threshold ϵ, i.e.,

$$\mathcal{L} = \left\{ l : \left| p\Big(l + \frac{g}{G} - \frac{l_i}{G}\Big)\right| > \epsilon \right\} \tag{8}$$

Letting $r^{(g)}[q] = r(qT_s + gT_s/G)$, $h^{(g)}[q,l] = h(qT_s + \frac{g}{G}T_s, l)$ and $w^{(g)}[q] = w(qT_s + \frac{g}{G}T_s)$, we can express (6) as

$$r^{(g)}[q] = \sum_{l\in\mathcal{L}} h^{(g)}[q,l]s[q-l] + w^{(g)}[q], \tag{9}$$

which forms the discrete-time received vector at g-th phase as $\mathbf{r}^{(g)} = [r^{(g)}[0], \ldots, r^{(g)}[MN-1]] \in \mathbb{C}^{MN\times 1}$, and the noise samples $w^{(g)}[q]$ are correlated due to ovesampling.

Using DZT on vector $\mathbf{r}^{(g)}$ yields the g-th phase received DD matrix $\mathbf{Y}^{(g)} \in \mathbb{C}^{M\times N}$ as

$$\mathbf{Y}^{(g)} = \Big[\mathbf{y}_0^{(g)}, \ldots, \mathbf{y}_{M-1}^{(g)}\Big]^T = \mathrm{vec}^{-1}\Big(\mathbf{r}^{(g)}\Big)\mathbf{F}_N = \tilde{\mathbf{Y}}^{(g)}\mathbf{F}_N, \tag{10}$$

where $\mathbf{y}_m^{(g)} = [\mathbf{Y}^{(g)}[m,0], \ldots, \mathbf{Y}^{(g)}[m,N-1]]^T \in \mathbb{C}^{N\times 1}$ is the received DD vector, and $\tilde{\mathbf{Y}}^{(g)} \in \mathbb{C}^{M\times N}$ is the received DT matrix at g-th phase expressed as

$$\tilde{\mathbf{Y}}^{(g)} = \Big[\tilde{\mathbf{y}}_0^{(g)}, \ldots, \tilde{\mathbf{y}}_{M-1}^{(g)}\Big]^T = \mathrm{vec}^{-1}\Big(\mathbf{r}^{(g)}\Big). \tag{11}$$

Here, $\tilde{\mathbf{y}}_m^{(g)} = [\tilde{\mathbf{Y}}^{(g)}[m,0], \ldots, \tilde{\mathbf{Y}}^{(g)}[m,N-1]]^T \in \mathbb{C}^{N\times 1}$ is the received g-th phase DT vector at m-th delay index.

By adopting zero-padding for OTFS with receiver oversampling as in [15], and utilizing $q = m + nM$ in (9), the vectorized DT domain input-output relation at g-th phase can be derived as

$$\tilde{\mathbf{y}}_m^{(g)} = \sum_{l\in\mathcal{L}} \tilde{\boldsymbol{\nu}}_{m,l}^{(g)} \circ \tilde{\mathbf{x}}_{m-l} + \tilde{\mathbf{w}}_m^{(g)}, \tag{12}$$

where $\tilde{\boldsymbol{\nu}}_{m,l}^{(g)} = [\tilde{\boldsymbol{\nu}}_{m,l}^{(g)}[0], \ldots, \tilde{\boldsymbol{\nu}}_{m,l}^{(g)}[N-1]]^T$ is the l-th tap DT channel vector at m-th delay index with g-th phase, with elements

$$\tilde{\boldsymbol{\nu}}_{m,l}^{(g)}[n] = \sum_{i=0}^{L-1} h_i e^{j\frac{2\pi}{MN}k_i\left(m+\frac{g}{G}-\frac{l_i}{G}\right)} e^{j\frac{2\pi}{N}k_i n} \times p\Big(l + \frac{g}{G} - \frac{l_i}{G}\Big) \tag{13}$$

for $n \in [0, N-1]$.

Applying FFT on (12) yields the corresponding DD domain input-output relation

$$\mathbf{y}_m^{(g)} = \frac{1}{\sqrt{N}} \sum_{l\in\mathcal{L}} \boldsymbol{\nu}_{m,l}^{(g)} \circledast \mathbf{x}_{m-l} + \breve{\mathbf{w}}_m^{(g)}, \tag{14}$$

$$= \sum_{l\in\mathcal{L}} \mathbf{K}_{m,l}^{(g)}\mathbf{x}_{m-l} + \breve{\mathbf{w}}_m^{(g)}, \tag{15}$$

where $\boldsymbol{\nu}_{m,l}^{(g)} = \mathbf{F}_N\tilde{\boldsymbol{\nu}}_{m,l}^{(g)}$ and $\mathbf{K}_{m,l}^{(g)} = \frac{1}{\sqrt{N}}\ \mathrm{circ}(\boldsymbol{\nu}_{m,l}^{(g)})$.

Delay Time MRC Detection: We apply the low complexity iterative DT MRC detector together with noise whitening to improve the performance as in [15]. Let us define the residual error term $\Delta\tilde{\mathbf{y}}_{\mathrm{wf}\ m}^{(g)}$, obtained through interference cancellation from the noise-whitened received signal using erroneous symbol estimates as

$$\Delta\tilde{\mathbf{y}}_{\mathrm{wf}\ m}^{(g)} = \tilde{\mathbf{y}}_{\mathrm{wf}\ m}^{(g)} - \sum_{l\in\mathcal{L}} \tilde{\boldsymbol{\nu}}_{\mathrm{wf}\ m,l}^{(g)} \circ \Big(\hat{\tilde{\mathbf{x}}}_{m-l}\Big), \tag{16}$$

where $\tilde{\mathbf{y}}_{\mathrm{wf}\ m}^{(g)}$ and $\tilde{\boldsymbol{\nu}}_{\mathrm{wf}\ m,l}^{(g)}$ are the DT received symbol and channel vector, respectively, after noise whitening. The MRC detector is initialized with the DT matrix $\hat{\tilde{\mathbf{X}}}^{(0)}$ and the residual error vector $\Delta\tilde{\mathbf{y}}_{\mathrm{wf}\ m}^{(0,g)}, \forall m \in [0, M-1]$ is calculated using (16). The detector then adopts following operations at i-th iteration

$$\tilde{\mathbf{d}}_m^{(i)} = \hat{\tilde{\mathbf{x}}}_m^{(i)} + \Delta\tilde{\mathbf{c}}_m^{(i)} \oslash \tilde{\mathbf{u}}_m, \tag{17}$$

forming $\tilde{\mathbf{D}}^{(i)} = [\tilde{\mathbf{d}}_0^{(i)}, \ldots, \tilde{\mathbf{d}}_{M-1}^{(i)}]^T$ for next iteration, where

$$\Delta\tilde{\mathbf{c}}_m^{(i)} = \sum_{g=0}^{G-1}\sum_{l\in\mathcal{L}} \Big(\tilde{\boldsymbol{\nu}}_{\mathrm{wf}\ m+l,l}^{(g)}\Big)^H \circ \Delta\tilde{\mathbf{y}}_{\mathrm{wf}\ m+l}^{(i,g)}, \tag{18}$$

$$\Delta\tilde{\mathbf{y}}_{\mathrm{wf}\ m+l}^{(i,g)} = \Delta\tilde{\mathbf{y}}_{\mathrm{wf}\ m+l}^{(i-1,g)} - \tilde{\boldsymbol{\nu}}_{\mathrm{wf}\ m+l,l}^{(g)} \circ \Big(\hat{\tilde{\mathbf{x}}}_m^{(i)} - \hat{\tilde{\mathbf{x}}}_m^{(i-1)}\Big), \tag{19}$$

$$\tilde{\mathbf{u}}_m = \sum_{g=0}^{G-1}\sum_{l\in\mathcal{L}} \Big(\tilde{\boldsymbol{\nu}}_{\mathrm{wf}\ m+l,l}^{(g)}\Big)^H \circ \tilde{\boldsymbol{\nu}}_{\mathrm{wf}\ m+l,l}^{(g)}. \tag{20}$$

Here, $\tilde{\mathbf{d}}_m^{(i)}$ in (17) denotes the soft estimate of $\hat{\tilde{\mathbf{x}}}_m^{(i)}$. For a comprehensive understanding of MRC detection with noise whitening, please refer to our work in [15].

Alternatively, to further improve the performance and reduce the number of iterations in MRC detector, a turbo iteration can be adopted. In the turbo iteration, the soft decision $\tilde{\mathbf{D}}^{(i)}$ are transformed into the DD domain through M parallel N-FFT operation which is subsequently passed through the QAM log likelihood ratio (LLR) detection followed by de-interleaver and LDPC decoder (see Fig. 1). The LDPC decoder generates the information bits along with the hard decisioned coded bits which are then interleaved and QAM modulated to obtain estimated DD $\hat{\mathbf{X}}$. By applying M parallel N-IFFT, it is converted to DT domain $\hat{\tilde{\mathbf{X}}}$ for use in the next iteration of MRC with a weighted sum of the hard and soft decision using weighting coefficient $\bar{\delta}$ as

$$\hat{\tilde{\mathbf{X}}}^{(i)} = \bar{\delta}\mathcal{F}\Big(\tilde{\mathbf{D}}^{(i)}\mathbf{F}_N\Big)\mathbf{F}_N^H + \big(1-\bar{\delta}\big)\tilde{\mathbf{D}}^{(i)}, 0 < \bar{\delta} \le 1, \tag{21}$$

where $\mathcal{F}(\cdot)$ encompasses a series of operations, including QAM LLR demodulator, de-interleaver, LDPC decoder, interleaver, and QAM modulator [17], [18], [19], [20] (see Fig. 1). Due to the computationally intensive nature of the operations of the turbo iteration $\mathcal{F}(\cdot)$, it is applied only after a certain number MRC detection iterations. The number of MRC iterations between each turbo iteration can be determined with a case-by-case optimization.

III. Different Reconstruction Filter

In this section, we discuss different D/A reconstruction filters, and analyze them in terms of spectral efficiency and OOB radiation. The OOB for the underlying system can be analyzed through power spectral density (PSD) at frequencies $m\Delta f$, $m = 0, \ldots, M-1$, as[1]

$$\begin{aligned}\mathbf{S}_{\mathrm{f}}[m] &= \mathrm{PSD}(f)|_{f=m\Delta f} \\ &= \frac{1}{NG}\sum_{g=0}^{G-1}\sum_{n=0}^{N-1}\mathbb{E}_{\mathbf{X}}\left|\mathbf{X}_{\mathrm{tf}}[mG+g,n]\right|^2,\end{aligned}$$

where $\mathbf{X}_{\mathrm{tf}} = \mathbf{F}_{MG}\cdot \mathrm{vec}^{-1}_{MG,N}(\mathbf{s}') \in \mathbb{C}^{MG\times N}$ is the oversampled time-frequency matrix and

$$\mathbf{s}' = \left\{\mathbf{s}\left(qT_s + \frac{gT_s}{G}\right)\right\}_{\substack{q=0,\ldots,MN-1\\ g=0,\ldots,G-1}} \in \mathbb{C}^{MGN\times 1} \quad (22)$$

is the oversampled discrete-time transmit signal.

A. Sinc Reconstruction Filter

Assuming a Sinc transmit reconstruction filter with impulse response $p_{\mathrm{tx}}(t)$, the receiver matched filter and the equivalent filter response $p(t)$ are Sinc, i.e.,

$$p_{\mathrm{tx}}(t) = p_{\mathrm{rx}}(t) = p(t) = \frac{\sin(\pi t)}{\pi t} = \mathrm{Sinc}(t). \quad (23)$$

The Sinc reconstruction filter offers precise control over the bandwidth of the reconstructed analog signal so that it occupies exactly $B_{\mathrm{Sinc}} = B$ bandwidth. However, an ideal Sinc filter is not realizable in practice, thus we use a truncated reconstruction filter with limited span which introduces some OOB leakage, i.e., $B_{\mathrm{TSinc}} \geq B$.

With the Sinc reconstruction filter, the spectral efficiency for the coded OTFS system is $\eta = \frac{R\cdot R_c}{B_{\mathrm{Sinc}}}$, where $R = \log_2(Q)f_s = \frac{\log_2(Q)}{T_s}$ denotes the bit rate. For the truncated Sinc (TSinc) filter, the spectral efficiency can be obtained by replacing B_{Sinc} by B_{TSinc} in the above computation of η.

B. Root Raised Cosine Reconstruction Filter

For the RRC transmit reconstruction filter, the matched filter is also an RRC, resulting in the equivalent filter $p(t)$ to be a raised cosine (RC) filter, given by

$$p(t) = \begin{cases} \frac{4}{\pi T_s}\,\mathrm{sinc}\left(\frac{1}{2\alpha}\right), & t = \pm\frac{1}{2\alpha} \\ \frac{1}{T_s}\,\mathrm{sinc}(t)\frac{\cos(\pi\alpha t)}{1-(\pi\alpha t)^2}, & \text{otherwise}\end{cases} \quad (24)$$

where α denotes the roll-off factor.

[1]Note that our OOB is based on the PSD per block, different from [21] using PSD per frame with zero paddings.

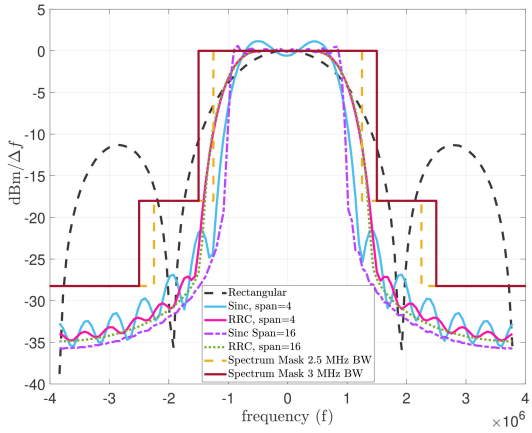

Fig. 2. OOB/block ($\mathbf{S}_{\mathrm{f}}[m]$) for different D/A reconstruction filters.

The RRC transmit filter leads to a bandwidth expansion $B_{\mathrm{RRC}} = (1+\alpha)B$. Thanks to its finite time duration and bandwidth of RRC filter, in practice, the OOB leakage for RRC filter is considerably smaller compared to the truncated Sinc filter. Spectral efficiency for a system utilizing the RRC D/A reconstruction filter is given by $\eta = \frac{R\cdot R_c}{B_{\mathrm{RRC}}}$.

In the next section, we will compare systems using the above filters and rectangular one, in terms of BERs and OOB. To make a fair comparison, we need to keep the same spectral efficiency across all systems by varying either R, R_c or bandwidth.

The rectangular D/A reconstruction filter (zero-order hold) satisfies the 3-dB bandwidth constraint but the OOB emission vastly exceeds the spectrum Mask (see discussion on Fig. 2 in the next Section).

IV. Results and Discussions

An OTFS system with $M = 128$ subbands spaced at $\Delta f = 15$ KHz, and $N = 128$ blocks in an OTFS frame is considered for the simulation. An oversampling factor of $G = 4$ is employed at the receiver. We adopt the 9-path EVA channel [22] with channel taps $|\mathcal{L}| = 8$ to capture 98 % of channel power at a speed of 500 kmph.

We plot PSDs per block for the truncated Sinc and RRC filters using $\mathbf{S}_{\mathrm{f}}[m]$ and compare them in Fig. 2 to assess the OOB performance. Both filters are configured with span settings of 4 and 16, and the number of symbols per sample is taken as 4. The roll off factor of RRC filter is 0.5. We also plot the spectrum emission mask [23] for two different channel bandwidths, 3 MHz and 2.5 MHz. The figure depicts that, with a span of 16, the main lobe of the truncated Sinc filter remains well-contained within the 2.5 MHz spectrum mask, whereas the RRC filter requires a broader 3 MHz bandwidth due to roll off. Further, a lower filter span could reduce the implementation complexity, but it comes at the cost of a slightly wider bandwidth.

We also observe that the OOB emission of the Sinc filter is higher than the RRC filter when using a lower filter span of 4, due to the larger truncation involved in its implementation. As expected, the OOB emission surpasses the RRC filter at higher spans. Additionally, we find that the rectangular filter performs the worst in terms of main lobe bandwidth confinement and OOB emission.

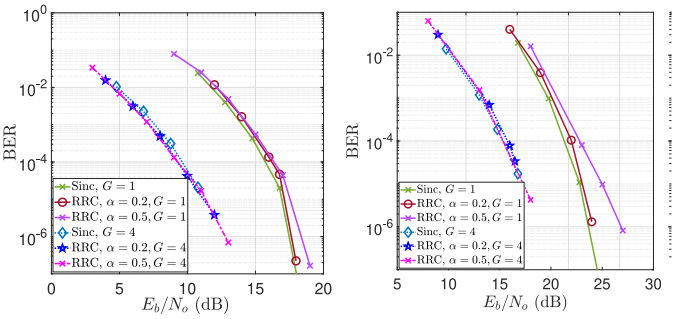

Fig. 3. BER vs E_b/N_0 comparison with different filters for 4-QAM (left) and 16-QAM (right).

In the following simulations, we evaluate the BER performance of coded OTFS, where the LDPC code has code length $N_c = 3072$, and number of codewords in each OTFS frame is $\lfloor (MN - |\mathcal{L}|N)/N_c \rfloor = 5$. We define $E_b/N_0\,(\text{dB}) = \text{SNR}(\text{dB}) - 10\log 10(R_c)$ for different R_c.

Fig. 3 shows BER vs E_b/N_0 of the coded OTFS system employing MRC detection for different D/A reconstruction filters with 4-QAM and 16-QAM signaling and MRC iterations of 3 and 5, respectively. The number of turbo iteration is set to 1 in all cases to limit complexity. The performance is obtained for receiver oversampling with noise whitening [15] as well as without oversampling. For fair comparison between the Sinc and RRC filters, we set the same spectral efficiency for both, and accordingly, choose code rate $R_c = \frac{1}{3}$ for Sinc, $R_c = \frac{2}{5}$ for RRC with $\alpha = 0.2$, and $R_c = \frac{1}{2}$ for RRC with $\alpha = 0.5$.

We observe that the MRC detector with receiver oversampling integrated with noise whitening outperforms the Nyquist sampling for all cases. The receiver oversampling improves the delay resolution by the oversampling factor G, resolving a larger number of distinct paths, and collecting G times more (correlated) observations. Noise whitening is used to de-correlate the noise components within these observations. Hence, the combination of oversampling and noise whitening can increase the diversity gain for MRC detection (see (17)-(20)), leading to significant performance enhancement. Furthermore, both Sinc and RRC (for all α's) filters exhibit nearly identical performance with oversampling. However, for Nyquist sampling, the MRC using Sinc filter outperforms RRC at $\alpha = 0.5$ by 0.5 dB and 2 dB for 4 and 16-QAM, at $\text{BER} = 10^{-5}$, since RRC decays faster than Sinc leading to reduced diversity. The decay in the RRC filter with $\alpha = 0.2$ is slower, hence it has better performance than RRC at $\alpha = 0.5$ but slightly degraded performance compared to the Sinc filter.

Therefore, we conclude that Sinc filter is a better choice compared to RRC, especially for larger α, in terms of both BER and bandwidth requirement under the same spectral efficiency.

V. Conclusion

In this letter, we consider a coded OTFS system using Sinc and RRC D/A reconstruction filters with the oversampling receiver. We provide, for the first time, a fair comparison of such systems in terms of bandwidth expansion, spectral efficiency and OOB leakage. For this, we fix the same spectral efficiency and accordingly adjust the code rate and roll off factor. Our findings indicate that the Sinc filter, with a filter span of 4, satisfies the standard spectrum emission mask and is a superior choice over the RRC filter in terms of error performance and bandwidth requirement.

References

[1] R. Hadani et al., "Orthogonal time frequency space modulation," in *Proc. IEEE Wireless Commun. Net. Conf.*, San Francisco, CA, USA, 2017, pp. 1–6.

[2] Y. Hong, T. Thaj, and E. Viterbo, *Delay-Doppler Communications*. Amsterdam, The Netherlands: Elsevier, 2022.

[3] P. Raviteja, K. T. Phan, and Y. Hong, "Embedded pilot-aided channel estimation for OTFS in delay–Doppler channels," *IEEE Trans. Veh. Tech.*, vol. 68, no. 5, pp. 4906–4917, May 2019.

[4] W. Shen, L. Dai, J. An, P. Fan, and R. W. Heath, "Channel estimation for orthogonal time frequency space (OTFS) massive MIMO," *IEEE Trans. Signal Process.*, vol. 67, no. 16, pp. 4204–4217, Aug. 2019.

[5] H. B. Mishra, P. Singh, A. K. Prasad, and R. Budhiraja, "OTFS channel estimation and data detection designs with superimposed pilots," *IEEE Trans. Wireless Commun.*, vol. 21, no. 4, pp. 2258–2274, Apr. 2022.

[6] A. Thomas, K. Deka, P. Raviteja, and S. Sharma, "Convolutional sparse coding based channel estimation for OTFS-SCMA in uplink," *IEEE Trans. Commun.*, vol. 70, no. 8, pp. 5241–5257, Aug. 2022.

[7] P. Raviteja, K. T. Phan, Y. Hong, and E. Viterbo, "Interference cancellation and iterative detection for orthogonal time frequency space modulation," *IEEE Trans. Wireless Commun.*, vol. 17, no. 10, pp. 6501–6515, Oct. 2018.

[8] L. Xiang, Y. Liu, L.-L. Yang, and L. Hanzo, "Gaussian approximate message passing detection of orthogonal time frequency space modulation," *IEEE Trans. Veh. Tech.*, vol. 70, no. 10, pp. 10999–11004, Oct. 2021.

[9] T. Thaj and E. Viterbo, "Low complexity iterative rake decision feedback equalizer for zero-padded OTFS systems," *IEEE Trans. Veh. Tech.*, vol. 69, no. 12, pp. 15606–15622, Dec. 2020.

[10] T. Thaj, E. Viterbo, and Y. Hong, "General I/O relations and low-complexity universal MRC detection for all OTFS variants," *IEEE Access*, vol. 10, pp. 96026–96037, 2022.

[11] A. Naikoti and A. Chockalingam, "Low-complexity delay-doppler symbol DNN for OTFS signal detection," in *Proc. IEEE 93rd Veh. Tech. Conf.*, Helsinki, Finland, 2021, pp. 1–6.

[12] Z. Zhang, L. Heng, W. Qianli, and P. Fan, "A survey on low complexity detectors for OTFS systems detectors for OTFS systems," *ZTE Commun.*, vol. 4, no. 19, pp. 3–15, 2021.

[13] A. S. Bora, K. T. Phan, and Y. Hong, "Spatially correlated MIMO-OTFS for LEO satellite communication systems," in *Proc. IEEE Intern. Conf. Commun. Workshops*, 2022, pp. 723–728.

[14] Y. Ge, Q. Deng, P. C. Ching, and Z. Ding, "Receiver design for OTFS with a fractionally spaced sampling approach," *IEEE Trans. Wireless Commun.*, vol. 20, no. 7, pp. 4072–4086, Jul. 2021.

[15] P. Priya, E. Viterbo, and Y. Hong, "Low complexity MRC detection for OTFS receiver with oversampling," *IEEE Trans. Wireless Commun.*, vol. 23, no. 2, pp. 1459–1473, Feb. 2024.

[16] D. Tse and P. Viswanath, *Fundamentals of Wireless Communication*. Cambridge, U.K.: Cambridge Univ., 2005.

[17] B. Sklar, *Digital Communications: Fundamentals and Applications*. London, U.K.: Pearson, 2021.

[18] S. J. Johnson, *Iterative Error Correction: Turbo, Low-Density Parity-Check and Repeat-Accumulate Codes*. Cambridge, U.K.: Cambridge Univ., 2010.

[19] M. Matsumoto and T. Nishimura, "Mersenne twister: A 623-dimensionally equidistributed uniform pseudo-random number generator," *ACM Trans. Model. Comput. Simul. (TOMACS)*, vol. 8, no. 1, pp. 3–30, 1998.

[20] *5G; NR; Multiplexing and Channel Coding, Release 16, Version 16.2.0*, 3GPP Standard 38.212, 2020.

[21] M. Bayat and A. Farhang, "A generalized framework for pulse-shaping on delay-doppler plane," 2023, *arXiv:2311.06936*.

[22] *LTE; Evolved Universal Terrestrial Radio Access (E-UTRA); Base Station (BS) Radio Transmission and Reception, Release 14, Version 14.3.0*, 3GPP Standard 36.104, 2017.

[23] *5G NR; User Equipment (UE) Radio Transmission and Reception; Part 1: Range 1 Standalone, Release 15, Version 15.5.0*, 3GPP Standard 38.101-1, 2019.